Catalysis Today 160 (2011) 103–108

Contents lists available at ScienceDirect

Catalysis Today

journal homepage: www.elsevier.com/locate/cattod

Au–Cu alloy nanoparticles supported on silica gel as catalyst for CO oxidation: Effects of Au/Cu ratios

Xiaoyan Liu[a,c], Aiqin Wang[a], Tao Zhang[a,*], Dang-Sheng Su[b], Chung-Yuan Mou[c,*]

[a] State Key Laboratory of Catalysis, Dalian Institute of Chemical Physics, Chinese Academy of Sciences, Zhongshan Road 457, Dalian 116023, PR China
[b] Fritz-Haber Institute of the Max Planck Society, Berlin D-14195, Germany
[c] Department of Chemistry, National Taiwan University, 1 Roosevelt Road, Sec 4, Taipei 106, Taiwan

ARTICLE INFO

Article history:
Available online 16 June 2010

Keywords:
Au–Cu alloy
Gold
Copper
Nanoparticle
CO oxidation
PROX

ABSTRACT

Au–Cu bimetallic catalysts with Au/Cu ratios ranging from 3/1 to 20/1 were prepared on silica gel support by a two-step method. The catalysts were characterized by ICP, XRD and TEM. The results showed that, irrespective of Au/Cu ratios, all the bimetallic nanoparticles had significantly reduced particle sizes (3.0–3.6 nm) in comparison with monometallic gold catalysts (5.7 nm). Both CO oxidation and PROX reactions were employed to evaluate the catalytic activities of Au–Cu bimetallic catalysts. For CO oxidation, the alloy catalysts show non-monotonic temperature dependence showing a valley in the intermediate temperature range. The catalyst with Au/Cu ratio of 20/1 gave the highest activity at room temperature, but its activity showed the deepest valley with increasing the reaction temperature. On the other hand, the catalyst with Au/Cu ratio of 3/1 exhibited the best performance for PROX reaction. For the Au/Cu ratios investigated, the bimetallic catalysts showed superior performance to monometallic gold catalysts, demonstrating the synergy between gold and copper.

© 2010 Elsevier B.V. All rights reserved.

1. Introduction

Gold nanocatalysts have been intensively studied since the pioneering work of Haruta in the 80 s of last century [1–3]. It has been reported that the optimized size of gold nanoparticles in CO oxidation reaction is ~3 nm [4–6]. Generally, highly dispersed gold nanoparticles can be facilely obtained by a deposition-precipitation (DP) method on "active" metal oxide supports (e.g., TiO_2, Fe_2O_3, etc.) with iso-electronic points (IEP) between 6 and 9 [7,8]. However, it remains challenging to obtain small gold nanoparticles on "inert" supports with acidic surfaces (e.g., silica, IEP = 2.0) and without anchoring sites (e.g., defects, F centers) [9,10]. At the same time, silica is appealing as a support for its large surface area, good thermal stability, high resistance against corrosion, and availability. Therefore, it would be attractive to synthesize highly dispersed and highly active gold nanocatalysts supported on silica.

It has been demonstrated theoretically that the electronic and structural properties of gold nanoparticles can be modified by doping with a second metal [11]. Supported bimetallic catalysts containing gold is becoming an emerging research subject recently, especially Au–platinum group metals (PGMs). It has been reported that supported Au–Pt bimetallic catalysts showed enhanced activity in methanol electrooxidation [12], oxygen reduction [13], CO tolerance for hydrogen activation [14] and biomass conversion [15]. Supported Au–Pd catalysts also showed superior activity compared to Au and Pd nanocatalysts in the acetoxylation of ethylene to vinyl acetate [16], alcohol oxidation [17] and direct synthesis of hydrogen peroxide [18]. Recently, supported Au–Ir bimetallic catalysts were reported to exhibit higher activity in CO oxidation than the monometallic ones [19]. However, alloying gold with the other two coinage metals (silver and copper) has received relatively less attention.

The group IB metals (gold, silver and copper) have the same face center cubic (fcc) crystal structure and similar lattice spacing, so they can form alloy very easily. In our previous work [20–23], we designed a one-pot method to prepare Au–Ag alloy nanoparticles supported on MCM-41. Gold and silver showed obvious synergetic effect in CO oxidation reaction. However, the particle size was not well controlled (~30 nm) and the Au–Ag@MCM-41 catalyst showed no activity when H_2 was present. Recently, we developed a general two-step method to prepare highly dispersed Au–Ag alloy nanoparticles on silica gel [24] and on MCM-41 [25] and Au–Cu alloy nanoparticles on SBA-15 [26]. It has been shown that alloying gold with silver or copper is a good way to obtain highly active, sintering-resistant nanoparticles on inert supports. For the Ag–Au alloy, the Au/Ag ratio was found to be a determining factor in the catalysts for the activity of CO oxidation [21]. The effect of Au/Cu ratios has not been investigated in details, in particular for large Au/Cu ratios. In this work, we prepared Au–Cu bimetallic catalysts

* Corresponding authors.
E-mail addresses: taozhang@dicp.ac.cn (T. Zhang), cymou@ntu.edu.tw (C.-Y. Mou).

0920-5861/$ – see front matter © 2010 Elsevier B.V. All rights reserved.
doi:10.1016/j.cattod.2010.05.019

with different Au/Cu ratios, from 3/1 to 20/1, with a focus on the effect of Au/Cu ratios on the particle size and catalytic activity for both CO oxidation and PROX reactions.

2. Experimental

2.1. Catalyst preparation

The Au–Cu alloy nanoparticles were supported on silica gel (provided by Qingdao Ocean Chemical Plant, $S_{BET} = 467\ m^2\ g^{-1}$) by a two-step method which was reported in our previous works [24–26]. Briefly, 1.0 g of the silica gel was dispersed in 50 mL ethanol containing 2.5 g of APTES ($H_2N(CH_2)_3Si(OEt)_3$) under stirring, and the mixture was then refluxed at 80 °C for 24 h. The recovered solid was dried at 60 °C overnight to obtain APTES-functionalized silica gel (APTES-SiO_2). To synthesize Au–Cu alloy nanoparticles supported on silica gel, in the first step, 1.0 g of the as-prepared APTES-SiO_2 was dispersed in 15 mL of H_2O, to which 5 mL of a 1.89 wt% $HAuCl_4$ aqueous solution was added. After continuous stirring at room temperature for 30 min, the mixture was recovered by filtration and washing, and was then redispersed in 20 mL of an aqueous solution of $NaBH_4$ (0.1 M) and stirred for another 20 min. After that, the solid was recovered by filtering and washing until there was no Cl^- detected by $AgNO_3$, thus obtaining Au/APTES-SiO_2. In the second step, Cu was deposited on the Au/APTES-SiO_2 using $Cu(NO_3)_2$ as the precursor with the same procedure as that for Au deposition in the first step. Finally, the solid was dried at 110 °C, calcined at 500 °C in air for 6 h, and reduced at 550 °C in pure H_2 for 1 h to obtain the Au–Cu/SiO_2 catalysts. The atomic ratio of gold to copper was varied from 3/1 to 20/1, and the total metal loading was fixed at 6 wt%. According to the nominal Au/Cu atomic ratios, the catalysts are designated as $Au_{20}Cu_1/SiO_2$, $Au_{10}Cu_1/SiO_2$, Au_6Cu_1/SiO_2, Au_3Cu_1/SiO_2, as well as Au/SiO_2 and Cu/SiO_2.

2.2. Characterization

The actual metal loadings of the catalysts were determined by inductively coupled plasma spectrometer (ICP-AES) on an IRIS Intrepid II XSP instrument (Thermo Electron Corporation). The wide-angle X-ray diffraction (XRD) patterns were recorded on a PW3040/60 X' Pert PRO (PANalytical) diffractometer equipped with a Cu K_α radiation source ($\lambda = 0.15432$ nm), operating at 40 kV and 40 mA. A continuous mode was used for collecting data in the 2θ range from 20° to 80° at a scanning speed of 5°/min. TEM images were obtained on a Tecnai G^2 Spirit FEI Transmission Electron Microscope operating at 120 kV. The particle size distribution of the catalysts was obtained by measuring more than 300 nanoparticles in each sample. The HRTEM images and the lattice parameters of the Au–Cu nanoparticles were observed with a Philips CM200 FEG electron microscope, operating at 200 kV and equipped with a Gatan GIF100 imaging filter.

2.3. Activity measurement

The catalytic testing was conducted with a continuous flow fixed-bed reactor system. Prior to the reaction, the catalyst was pretreated with H_2 at 550 °C for 1 h, and then cooled to the reaction temperature under He. For CO oxidation, the feed gas containing 1.0 vol% CO and 1.0 vol% O_2 balanced with He was allowed to pass through 60 mg (20–40 mesh) of a catalyst sample at a flow rate of 20 mL min^{-1} (corresponding to a space velocity of 20, 000 mL h^{-1} g_{cat}^{-1}). For preferential CO oxidation in rich H_2, the feed stream was composed of 1.0 vol% CO, 0.5 vol% O_2 and 50 vol% H_2 balanced with He, and the total flow rate was 40 mL min^{-1} (corresponding to a space velocity of 40, 000 mL h^{-1} g_{cat}^{-1}). The inlet and outlet gas compositions were analyzed on-line by a gas chromatograph (HP 6890, TDX-01 column).

3. Results and discussion

3.1. Actual Au/Cu molar ratios

In order to investigate the effect of Au/Cu ratios on the catalytic performance, we prepared four Au–Cu bimetallic catalysts with different Au/Cu atomic ratios according to our previously developed two-step approach [24–26]. As shown in Table 1, when the nominal Au/Cu ratios were 20/1 and 10/1, the actual Au/Cu ratios were almost exactly the same as the nominal values. However, for the nominal Au/Cu ratios of 6/1 and 3/1, the actual Au/Cu atomic ratios were somewhat larger than the nominal values. The deviation of the actual Au/Cu ratios from their nominal values at low Au/Cu ratios indicates that the loading of Cu on the support is more difficult than that of Au. Actually, comparing the metal loadings of Au/SiO_2 and Cu/SiO_2, one can see that the actual Cu loading is only one-third that of Au although their nominal loadings were all at 6 wt%. Apparently, the interaction between the amine ($-NH_2$) on the support surface and copper is weaker than with gold species.

3.2. Wide-angle XRD patterns

Fig. 1 presents the XRD patterns of the four bimetallic samples before and after the reduction treatment. Irrespective of the Au/Cu ratios, the four samples before the reduction treatment show the same XRD patterns as Au/SiO_2. None of any copper species, either copper oxides or metallic Cu, were detected by XRD. It is noted that even for the Cu/SiO_2 catalyst, not any copper crystal species were detected, suggesting that copper may exist as highly dispersed particles or amorphous species that could not be detected by XRD. On the other hand, upon reduction treatment with H_2, the XRD peaks slightly shift toward high angles with decreasing Au/Cu ratios, and this shift became more discernable at the Au/Cu ratio of 3/1. The d spacings, which were calculated according to the (1 1 1) reflection peak, also reflect such a tendency (Table 1). This is an indication of the formation of Au–Cu alloy after the reduction treatment [27]. The

Table 1
Chemical compositions, average particle sizes and the lattice spacings of Au–Cu/SiO_2 with various Au/Cu atomic ratios.

Catalysts	Au/Cu [a]	Total metal loading (wt%) [a]	D_{XRD} (nm)[b]	d spacing (nm)	D_{TEM} (nm) [c]	Specific rate (mol_{co} g_{Au}^{-1} h^{-1})	Contact time (g_{cat} h mol_{co}^{-1})	TOF (s^{-1})
Au/SiO_2	1/0	5.72	4.3	0.235	5.7	0.10	4.3	0.018
$Au_{20}Cu_1/SiO_2$	19.55/1	5.55	2.6	0.233	3.6	0.21	4.3	0.036
$Au_{10}Cu_1/SiO_2$	10.14/1	5.52	2.4	0.232	3.5	0.14	4.3	0.023
Au_6Cu_1/SiO_2	7.09/1	5.74	2.5	0.231	3.2	0.14	4.3	0.020
Au_3Cu_1/SiO_2	3.99/1	5.35	2.6	0.229	3.0	0.18	4.3	0.023
Cu/SiO_2	0/1	1.91	–	0.208	–	–	–	–

[a] Atomic ratios of Au to Cu determined by ICP.
[b] Average particle sizes estimated from Scherrer's equation according to XRD.
[c] Average particle sizes estimated by TEM images.

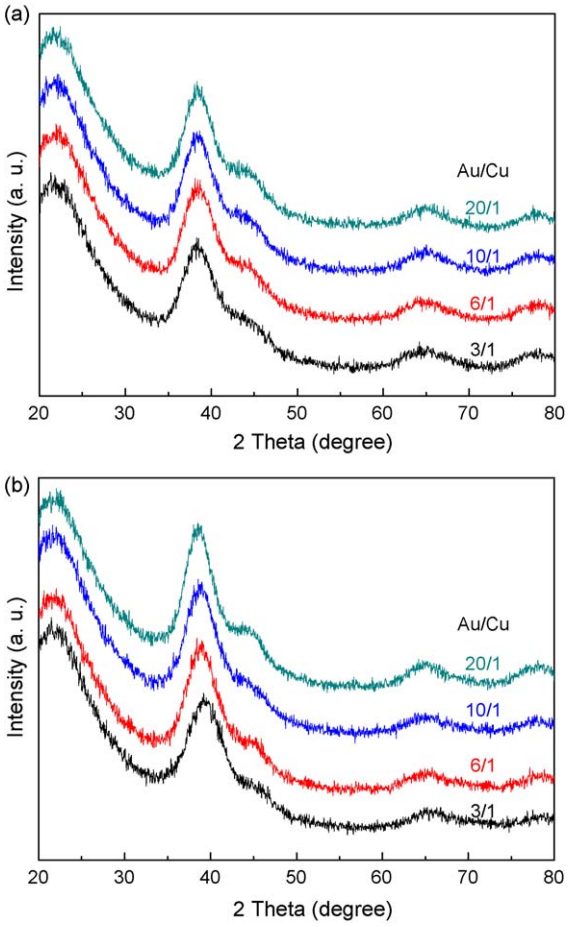

Fig. 1. XRD patterns of Au–Cu/SiO_2 catalysts with different Au/Cu atomic ratios: (a) calcined at 500 °C for 6 h in air; (b) sample (a) reduced at 550 °C for 1 h in pure H_2.

average particle sizes of the bimetallic catalysts, which were calculated by Scherrer's equation, are found to be almost invariant with respect to the Au/Cu ratios, and much smaller compared with that of Au/SiO_2 catalyst. This result indicates that the presence of Cu, even in a very small amount, prevent effectively the gold particles from sintering.

3.3. TEM and HRTEM images

Fig. 2 shows the TEM images and the corresponding particle size distributions of the four bimetallic catalysts. In agreement with the XRD examinations, the metal particles are found to be uniformly dispersed on the surface of the silica support. The average particle sizes are only slightly increased from 3.0 to 3.6 nm when the Au/Cu ratios are increased from 3/1 to 20/1. In comparison with the Au/SiO_2 catalyst which has the average particle size of 5.7 nm [24], all the Au–Cu bimetallic catalysts show significantly reduced particle sizes. In our previous work on Au–Ag bimetallic catalysts [24,25], we proposed a core–shell model to interpret the key role of Ag in limiting the aggregation of gold particles. Similarly, we propose copper oxide will form a shell on the gold nanoparticles so that they can inhibit the aggregation of gold particles during high-temperature calcination. However, at Au/Cu ratio of 20/1, the amount of copper is too small to form a monolayer on the gold core. In that case, the copper oxide may just form as some patches on the surface of gold core. The small patches of copper oxide may still play a key role in limiting the aggregation of gold particles. Upon reduction, the copper oxide species are reduced to metallic copper and the latter diffuse into the crystalline structure of gold to form Au–Cu alloy.

In order to confirm the formation of Au–Cu alloy upon reduction, we further performed HRTEM examination on the Au_3Cu_1/SiO_2 sample. The representative HRTEM image is shown in Fig. 3. The d spacings of the arbitrarily selected single nanoparticles are found to be 0.227, 0.228, and 0.233 nm, respectively; lying between the d spacings of monometallic Au (0.235 nm) and Cu (0.208 nm), suggesting that these particles are composed of random alloy of Au and Cu. In addition, we see that the d values differ from one particle to another, which may indicate that the composition of the Au–Cu alloy nanoparticles is fluctuating.

3.4. Catalytic activity for CO oxidation

Low-temperature CO oxidation is a good probe reaction to characterize the properties of gold-based catalysts. In the present work, Au–Cu bimetallic catalysts with various Au/Cu ratios were measured for CO oxidation. Fig. 4 illustrates the CO conversions as a function of the reaction temperature. First, as we have demonstrated in previous reports [24,25], SiO_2-supported gold catalyst presented a fairly good activity for low-temperature CO oxidation. The CO conversion attained ~50% even at below 0 °C. However, for Au/SiO_2 the conversion level remained roughly unchanged with increasing reaction temperature until 150 °C. The silica supported Au catalyst achieved a full conversion of CO only at a very high-temperature of 200 °C. This unusual behavior of Au/SiO_2 is very different from other gold catalysts, such as Au/TiO_2 [28] and Au/Fe_2O_3 [29], and the underlying cause is yet to be determined. In contrast, the Cu/SiO_2 sample gave a rather poor catalytic activity; the onset temperature is higher than 100 °C. Remarkably different from either Au/SiO_2 or Cu/SiO_2, the Au–Cu bimetallic catalysts present synergistic effect in catalysis between Au and Cu. Previously, Zhu et al. [30] also found enhanced performance in CO oxidation reaction when Cu and Au are deposited on TiO_2 nanotube. Apparently, Cu promoted the catalysis of Au on CO oxidation. The light-off temperature for the 100% CO conversion was 70 and 170 °C for Au–Cu/TiO_2 and Au/TiO_2, respectively.

For our bimetallic catalyst, irrespective of Au/Cu ratios, all the Au–Cu bimetallic catalysts gave similar CO conversions below 0 °C and a 100% CO conversion at 30 °C. Further increasing the reaction temperature from 30 to 200 °C brought about the appearance of a valley in the curve of CO conversions. Moreover, both the width and the depth of the valley depends on the Au/Cu ratios. The higher the Au/Cu ratio is, the deeper and wider is the valley. Such non-monotonic activity-reaction temperature dependence was also observed in our previously reported Au–Ag bimetallic system [21]. An important point to be noted is that the monometallic gold or copper do not exhibit such uncommon activity-reaction temperature curve. Therefore, the appearance of the activity valley may be linked with the modification of Au by Ag or Cu. In an investigation of Au catalyzed CO oxidation, Daté et al. [31] reported that the CO conversion decreased with increasing temperature when certain amount of moisture was added into the inlet gas. However, the dry inlet gas as well as the absence of the activity valley in Au/SiO_2 excludes the moisture effect in our work. On the other hand, Qian et al. [32] observed a similar activity-reaction temperature dependence over Au/ZnO/SiO_2–NH_3, and they attribute this behavior to the switching between two different reaction pathways, a low-temperature reaction pathway and high-temperature reaction pathway. In the low-temperature pathway, the weakly adsorbed species (either molecular oxygen or other key species related with oxygen activation) desorbs with increasing the reaction temperature, resulting in the loss of activity following this pathway. According to this model, we can imagine that the weakly adsorbed species must desorb much faster from the catalysts with

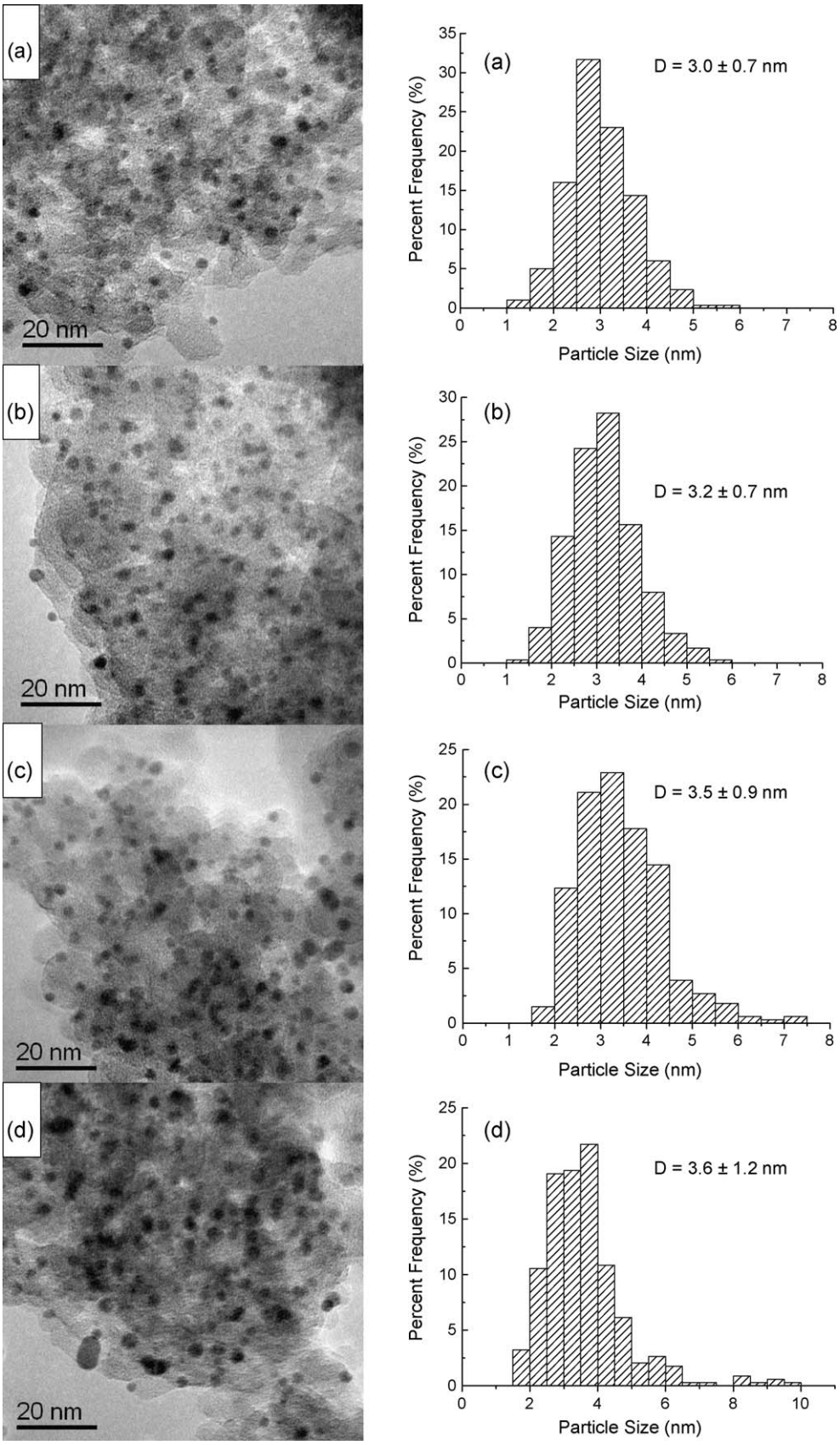

Fig. 2. TEM images and the corresponding particle size distributions of Au–Cu/SiO_2 catalysts with different Au/Cu atomic ratios: (a) 3/1, (b) 6/1, (c) 10/1 and (d) 20/1.

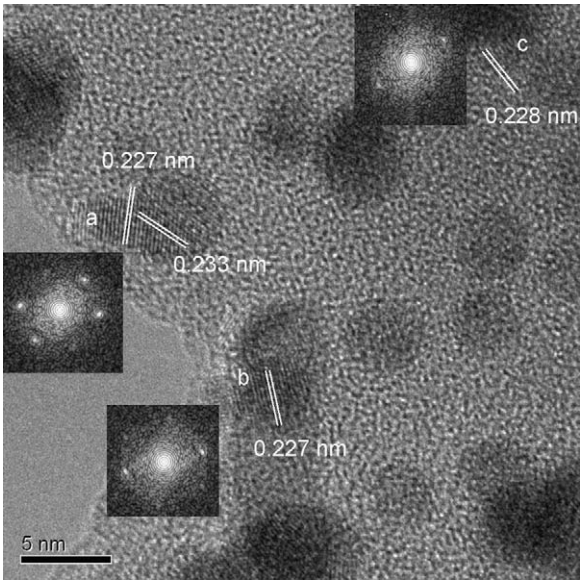

Fig. 3. HRTEM image and the lattice spacing of arbitrarily selected single nanoparticles of Au_3Cu_1/SiO_2.

higher Au/Cu ratios. This is reasonable assuming that the weakly adsorbed species is oxygen and the Cu species plays the important role in activating oxygen molecules.

To quantitatively compare the catalytic activity of Au–Cu catalysts with different Au/Cu ratios, we further measured the specific rates and TOFs (turnover frequencies) assuming that gold is the active site and Cu just acts as a promoter. Note that the measurement condition for specific rates and TOFs is different from that for conversion–temperature curves; the former is characterized by low CO conversions through diluting the catalyst with quartz sand or via increasing the flow rate. As shown in Table 1, the $Au_{20}Cu_1/SiO_2$ gives the highest specific rate and TOF among all the samples investigated when the reaction temperature was 30 °C. In other words, even a very little amount of Cu led to a substantial improvement in activity of gold. On the other hand, as demonstrated by XRD and TEM results, the sizes of bimetallic nanoparticles are almost independent on the Au/Cu ratios; even a very little amount of Cu could significantly limit the aggregation of gold. Hence, the superior activity of the $Au_{20}Cu_1/SiO_2$ for the low-temperature CO oxidation might be originated mainly from the electronic effect which is brought about by Cu. This result is reminiscent of nanoporous gold reported in literature [33–35]. In nanoporous gold, the residual silver content in the bulk was less than 1%, but the high catalytic activity of nanoporous gold was argued to be related to the presence of small amount of Ag where Ag was proposed to play a key role in activating oxygen [33–35]. Haruta proposed an inversely supported gold model for nanoporous gold where Ag_2O patches were dispersed on the surface of gold and the CO oxidation occurs at the perimeter interfaces at the junction between gold and Ag_2O [36]. Similar to Ag, Cu and its oxides are able to adsorb and activate oxygen. Therefore, in the case of Au–Cu bimetallic catalysts, we also

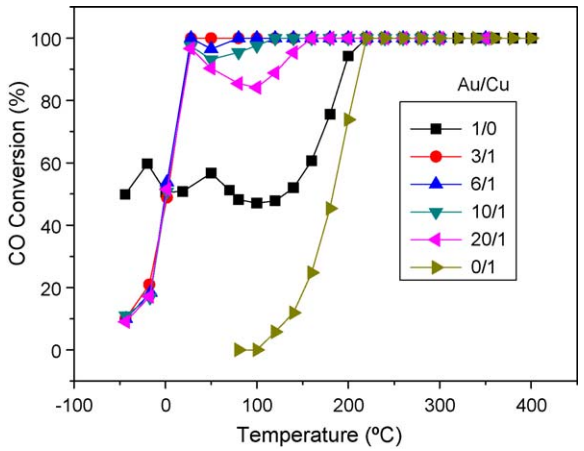

Fig. 4. CO conversions with reaction temperature over Au–Cu/SiO_2 with various Au/Cu atomic ratios. In each experiment, 60 mg of the catalyst was used. Gas mixture: $CO/O_2/He = 1/1/98$ (vol); flow rate: 20 mL min^{-1}.

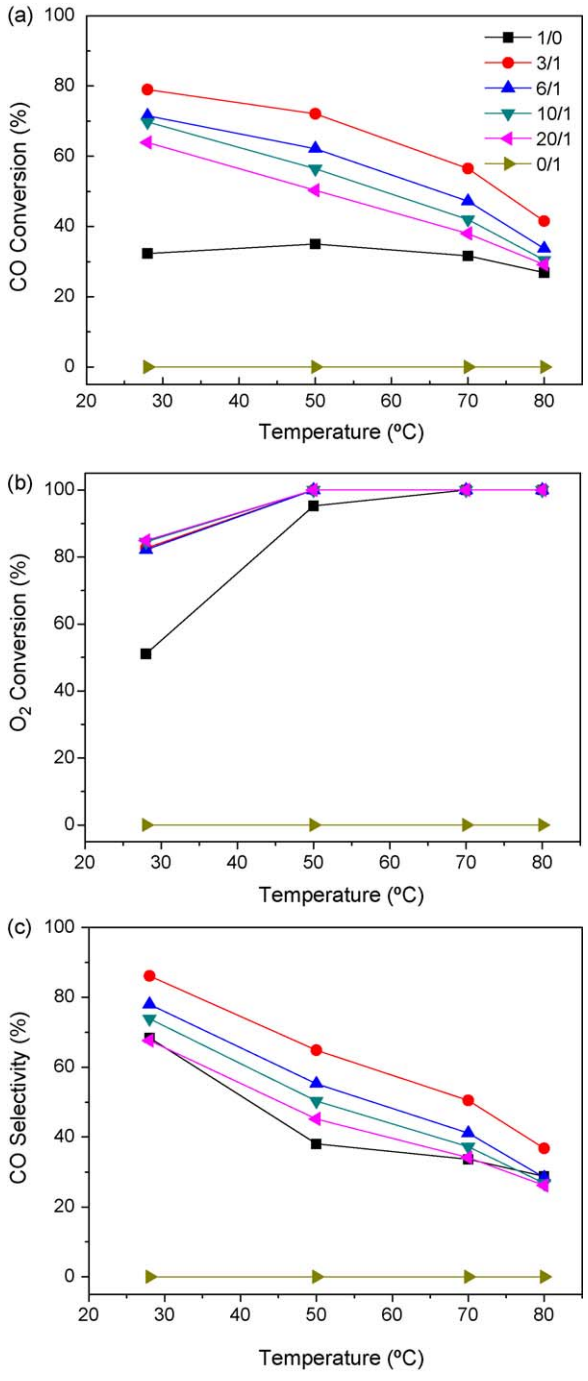

Fig. 5. CO conversions (a), O_2 conversions (b) and CO selectivities (c) with reaction temperature over Au–Cu/SiO_2 catalysts with various Au/Cu atomic ratios. In each experiment, 60 mg of the catalyst was used. Gas mixture: $CO/O_2/H_2/He = 1/0.5/50/48.5$ (vol); flow rate 40 mL min^{-1}.

propose that CO adsorbed on gold reacts with O activated on copper oxide to form CO_2. The higher activity of $Au_{20}Cu_1/SiO_2$ may suggest that highly dispersed copper or its oxides facilitate better oxygen activation.

3.5. Catalytic activity for preferential oxidation of CO in rich H_2

Preferential oxidation of CO is an important reaction for reducing the CO concentration in excess amount of hydrogen to an acceptable level for fuel cell operation. Fig. 5 shows the catalytic performances of Au–Cu bimetallic catalysts. Both the CO conversions and the CO_2 selectivities decrease with increasing the reaction temperature due to the competitive oxidation of H_2. Recently, Mozer et al. [37] found similar temperature trend in the selective carbon monoxide oxidation on a Au–Cu catalyst supported on alumina.

Comparing the catalysts with different Au/Cu ratios, both the CO conversions and the CO_2 selectivities increase with decreasing the Au/Cu ratios, while the oxygen conversions do not change with the Au/Cu ratios. Moreover, the Cu/SiO_2 sample did not exhibit any activity in this range of reaction temperature. The much higher O_2 conversions over the Au–Cu bimetallic catalysts than that over Au/SiO_2 also suggest that the Cu component in the Au–Cu catalysts facilitates the activation of oxygen at low-temperatures, which is very different from the Cu/SiO_2. Among the four Au–Cu bimetallic catalysts, the Au_3Cu_1/SiO_2 catalyst shows the best performance for PROX reaction. A point may be noted here, is that the reaction temperature range for PROX reaction, i.e., 27–80 °C is coincidently where the activity valley begins to take place in pure CO oxidation (see Fig. 4). In that temperature range, the activity for CO oxidation follows the order of $Au_3Cu_1/SiO_2 > Au_6Cu_1/SiO_2 > Au_{10}Cu_1/SiO_2 > Au_{20}Cu_1/SiO_2$. Obviously, the Cu component is exerting different influences on Au in the two reaction temperature range. Below room temperature, it appears that even a tiny amount of Cu is enough to promote the CO oxidation over gold. However, between RT and 200 °C, a higher amount of Cu is required to keep the high activity from decaying. In the future work, the reaction mechanisms involved in CO oxidation in these two reaction temperature range will be revealed by kinetic studies as well as in situ spectroscopy characterizations.

4. Conclusions

In summary, we have prepared Au–Cu bimetallic nanoparticles on silica gel support by a two-step method. Irrespective of Au/Cu ratios, the bimetallic nanoparticles are highly dispersed on the support and the particle sizes are significantly reduced in comparison with monometallic Au/SiO_2. The Au–Cu bimetallic nanoparticles showed higher catalytic activities than monometallic gold catalysts, for both CO oxidation and PROX reactions. Moreover, Cu influenced the catalytic activity of Au differently in two ranges of reaction temperatures. In the low reaction temperature range (<room temperature), even a tiny amount of Cu resulted in a very large increase of the reaction rate. However, in the temperature range of ~200 °C, an activity valley was clearly observed in Au–Cu bimetallic catalysts and the valley strongly depended on the Au/Cu ratios. The appearance of the activity valley suggests switching from one reaction mechanism to another, which deserves to be studied further.

Acknowledgement

Support from the National Natural Science Foundation of China (NNSFC 20773124) is gratefully acknowledged.

References

[1] M. Haruta, Catal. Today 36 (1997) 153.
[2] M.C. Daniel, D. Astruc, Chem. Rev. 104 (2004) 293.
[3] A. Stephen, K. Hashmi, G.J. Hutchings, Angew. Chem. Int. Ed. 45 (2006) 7896.
[4] M. Haruta, Chem. Rec. 3 (2003) 75.
[5] M.S. Chen, D.W. Goodman, Science 306 (2004) 252.
[6] H. Falsig, B. Hvolbæk, I.S. Kristensen, T. Jiang, T. Bligaard, C.H. Christensen, J.K. Nørskov, Angew. Chem. Int. Ed. 47 (2008) 4835.
[7] G.C. Bond, D.T. Thompson, Catal. Rev. Sci. Eng. 41 (1999) 319.
[8] M.M. Schubert, S. Hackenberg, A.C. van Veen, M. Muhler, V. Plzak, R.J. Behm, J. Catal. 197 (2001) 113.
[9] B.K. Min, W.T. Wallace, D.W. Goodman, Surf. Sci. 600 (2006) L7.
[10] Z. Yan, S. Chinta, A.A. Mohamed, J.P. Fackler, D.W. Goodman, J. Am. Chem. Soc. 127 (2005) 1604.
[11] H. Häkkinen, S. Abbet, A. Sanchez, U. Heiz, U. Landman, Angew. Chem. Int. Ed. 42 (2003) 1297.
[12] Y. Lou, M.M. Maye, L. Han, J. Luo, C.J. Zhong, Chem. Commun. (2001) 473.
[13] J. Zhang, K. Sasaki, E. Sutter, R.R. Adzic, Science 315 (2007) 220.
[14] S. Zhou, G.S. Jackson, B. Eichhorn, Adv. Funct. Mater. 17 (2007) 3099.
[15] G. Budroni, A. Corma, J. Catal. 257 (2008) 403.
[16] M. Chen, D. Kumar, C.W. Yi, D.W. Goodman, Science 310 (2005) 291.
[17] D.I. Enache, J.K. Edwards, P. Landon, B. Solsona-Espriu, A.F. Carley, A.A. Herzing, M. Watanabe, C.J. Kiely, D.W. Knight, G.J. Hutchings, Science 311 (2006) 362.
[18] J.K. Edwards, A.F. Carley, A.A. Herzing, C.J. Kiely, G.J. Hutchings, Faraday Discuss. 138 (2008) 225.
[19] A. Gómez-Cortés, G. Díaz, R. Zanella, H. Ramírez, P. Santiago, J.M. Saniger, J. Phys. Chem. C 113 (2009) 9710.
[20] J.H. Liu, A.Q. Wang, Y.S. Chi, H.P. Lin, C.Y. Mou, J. Phys. Chem. B 109 (2004) 40.
[21] A.Q. Wang, J.H. Liu, S.D. Lin, T.S. Lin, C.Y. Mou, J. Catal. 233 (2005) 186.
[22] A.Q. Wang, Y.P. Hsieh, Y.F. Chen, C.Y. Mou, J. Catal. 237 (2006) 197.
[23] A.Q. Wang, C.M. Chang, C.Y. Mou, J. Phys. Chem. B 109 (2005) 18860.
[24] X. Liu, A. Wang, X. Yang, T. Zhang, C.Y. Mou, D.S. Su, J. Li, Chem. Mater. 21 (2009) 410.
[25] C.W. Yen, M.L. Lin, A.Q. Wang, C.Y. Mou, J. Phys. Chem. C 113 (2009) 17831.
[26] X. Liu, A. Wang, X. Wang, C.Y. Mou, T. Zhang, Chem. Commun. (2008) 3187.
[27] S. Pal, G. De, J. Mater. Chem. 17 (2007) 493.
[28] F. Boccuzzi, A. Chiorino, M. Manzoli, P. Lu, T. Akita, S. Ichikawa, M. Haruta, J. Catal. 202 (2001) 256.
[29] M. Khoudiakov, M.C. Gupta, S. Deevi, Appl. Catal. A: Gen. 291 (2005) 151.
[30] B. Zhu, Q. Guo, S. Wang, X. Zheng, S. Zhang, S. Wu, W. Huang, React. Kinet. Catal. Lett. 88 (2006) 301.
[31] M. Daté, M. Okumura, S. Tsubota, M. Haruta, Angew. Chem. Int. Ed. 43 (2004) 2129.
[32] K. Qian, W. Huang, J. Fang, S. Lv, B. He, Z. Jiang, S. Wei, J. Catal. 255 (2008) 269.
[33] V. Zielasek, B. Jürgens, C. Schulz, J. Biener, M.M. Biener, A.V. Hamza, M. Bäumer, Angew. Chem. Int. Ed. 45 (2006) 8241.
[34] A. Wittstock, B. Neumann, A. Schaefer, K. Dumbuya, C. Kübel, M.M. Biener, V. Zielasek, H.P. Steinrück, J.M. Gottfried, J. Biener, A. Hamza, M. Bäumer, J. Phys. Chem. C 113 (2009) 5593.
[35] C. Xu, J. Su, X. Xu, P. Liu, H. Zhao, F. Tian, Y. Ding, J. Am. Chem. Soc. 129 (2007) 42.
[36] M. Haruta, ChemPhysChem 8 (2007) 1911.
[37] T.S. Mozer, D.A. Dziuba, C.T.P. Vieira, F.B. Passos, J. Power Source 187 (2009) 209.